A 5-km-thick reservoir with >380,000 km^3 of magma within the ancient Earth's crust

Rais Latypov (rais.latypov@wits.ac.za)
University of the Witwatersrand https://orcid.org/0000-0002-8158-5949
Sofya Chistyakova
University of the Witwatersrand
Richard Hornsey
Richard Hornsey Consulting (Pty) Ltd
Gelu Costin
Rice University https://orcid.org/0000-0003-3054-7886
Mauritz van der Merwe
retired

Physical Sciences - Article

Keywords:

Posted Date: December 9th, 2021

DOI: https://doi.org/10.21203/rs.3.rs-1104213/v1

Abstract

Several recent studies have argued that large, long-lived and molten magma chambers[1–10] may not occur in the shallow Earth's crust[11–23]. Here we present, however, field-based observations from the Bushveld Complex[24] that provide evidence to the contrary. In the eastern part of the complex, the magmatic layering was found to continuously drape across a ~4-km-high sloping step in the chamber floor. Such deposition of magmatic layering implies that the resident melt column was thicker than the stepped relief of the chamber floor. Prolonged internal differentiation within such a thick magma column is further supported by evolutionary trends in crystallization sequence and mineral compositions through the sequence. The resident melt column in the Bushveld chamber during this period is estimated to be >5-km-high in thickness and >380,000 km^3 in volume. This amount of magma is three orders of magnitude larger than any known super-eruptions in the Earth's history[25] and is only comparable to the extrusive volumes of some of Earth's large igneous provinces[26]. This suggests that super-large, entirely molten and long-lived magma chambers, at least occasionally, occur in the geological history of our planet. Therefore, the classical view of magma chambers as 'big magma tanks'[1–10] remains a viable research concept for some of Earth's magmatic provinces.

Full Text

For over a century, the classic paradigm of volcanology and igneous petrology has been premised upon the existence of magma chambers, filled by crystal-free melt, like 'big tanks'[1–10]. Such magma chambers gradually lose heat and crystallize from all margins inwards and occasionally supply overlying extrusive centres (volcanoes or fissures) with melts that erupt onto the Earth's surface[1–10]. This founding concept has been, however, recently challenged on the basis of observations and evidence from various disciplines. The most often-cited evidence is derived from geophysical surveys that are unable to conclusively identify any present-day magma chambers with large volumes of eruptible melt[27]. This is supported by thermal modelling, which indicates that the formation of a large magma body within the upper crust is physically problematic, because it requires a magma accumulation rate that is 1-2 orders of magnitude greater than determined through geochronology[27]. In addition, out-of-sequence geochronology was used to argue that the mafic-ultramafic plutons do not require the existence of large magma chambers but can rather be produced as a stack of randomly-emplaced and amalgamated sills[19,20,23]. The conclusion from these studies is that large and mostly molten magma chambers are likely either transient[14] or non-existent[11,12] in the geological history of Earth. As an alternative, it is proposed that all the melt is stored within intergranular pockets of crystal-rich mushes that occupy almost the entire crust, from its Moho towards the surface[13–15,17,18,28]. The periodic tectonic destabilization of the mush may produce small, discrete melt lenses that subsequently aggregate, ascend and erupt as lava. There are, however, some observations from magmatic complexes[29] and thermal modelling constraints[30] that come into conflict with this emerging paradigm[13–15,17,18,28]. Here we present one clear-cut case from the Bushveld Complex whose magma chamber appears to have contained, during one stage of its evolution,

an enormous volume of resident melt that slowly crystallized from the base upwards to produce a continuous sequence of chemically stratified cumulate rocks.

Incremental growth of the Bushveld Complex

The 2.05 billion-year-old Bushveld Complex in South Africa is the largest mafic-ultramafic layered intrusion into the Earth's crust. It occupies an area that most likely exceeds 100,000 km^2 and extends ~450 km east-west and ~350 km north-south[24,31–33]. Despite its enormous size, this complex is merely the remaining portion of an originally much larger intrusion that has subsequently been eroded to an unknown extent by surface processes. The complex consists of several parts, of which the western, eastern and northern limbs are the largest, and is stratigraphically subdivided into five major units - the Marginal, Lower, Critical, Main, and Upper Zones, comprising a total thickness of about 7 to 9 km[24]. The Bushveld Complex is widely considered to be a typical example of an open-system magma chamber[34]. Apart from the marginal rocks, its four principal zones are attributed to major replenishing events, with numerous smaller magma recharges contributing to the formation of these zones. During this process, the magma chamber incrementally increased in size through both vertical and lateral inflation[34–36]. All major replenishing events are marked by regionally extensive magmatic disconformities, local erosive unconformities into previous strata, significant isotopic shifts, and notable changes in whole-rock and mineral compositions[34]. These relationships are best exemplified by the Main Zone (MZ) at the Tonteldoos area of the southeastern Bushveld Complex (Fig. 1), which has a much larger lateral extent than its underlying Critical Zone (CZ), as indicated by the MZ's direct onlapping of the floor rocks in many places. The MZ is commonly attributed to a large influx of new magma that significantly expanded the chamber in both vertical and lateral extent, producing a regional disconformity[34] and locally prominent unconformities with pre-existing CZ cumulates[37]. The base of the MZ is also marked by a substantial isotopic shift towards more radiogenic whole-rock $^{87}Sr/^{86}Sr$ ratios[38]. The laterally extensive Pyroxenite Marker in the uppermost part of the MZ indicates another major expansion of the chamber through a magma replenishment and mixing event that caused an isotopic shift towards less radiogenic whole-rock $^{87}Sr/^{86}Sr$ ratios[39,40] and an increase in both the An-content of plagioclase and Mg-number of pyroxenes[41–44].

The resident melt column of the Bushveld Complex

The stratigraphy of the Bushveld Complex is most commonly thought to have progressively accumulated from the overlying resident melt by deposition of crystals on the chamber floor[6,34,45] althought there are some alternative views[19,21,23]. A critical unknown parameter is the volume of resident melt at any particular time during the evolution of the magma chamber[31,46]. We present here a potential solution to this issue through field mapping of the southeastern Bushveld Complex in the Tonteldoos area (Fig. 2), where the resident melt column thickness at the time of MZ crystallization may be assessed. The field mapping and 1:250,000 scale regional geology maps of the study area are compiled into a 3D model that includes and respects all mapped relationships between various geological units. The along-strike section

in Fig. 2 is viewed down the dip of the stratigraphy and thereby preserves all the relationships between the intrusion and its host rocks, without loss of any details. It reveals that the host stratigraphy along this section dips at 10° to the west. The sedimentary host rock sequence was injected by Bushveld-related sills that are sharply truncated by the Bushveld Complex. The mapped geology exposes no evidence for any post-emplacement structural deformations, implying that the section was emplaced as shown and preserves all primary igneous field relationships.

Two notable features in Fig. 2 provide crucial constraints. The first relates to the geometry of the chamber that has been previously subdivided and called as two large basinal structures[41]. We refer to them here, however, as the Roossenekal and Belfast sub-chambers because they lack any associated structural deformation or down-warping of their sedimentary host rocks (Fig. 2). The floors to both sub-chambers are concave upwards and juxtapose an intervening Stoffberg remnant of non-deformed host rocks. The floor contact of the Roossenekal sub-chamber has an impressive ~6-km-high shelf relief (termed the Tonteldoos step; Fig. 2b) with a ~10° slope across ~35 km up to the summit of the Stoffberg remnant. This topographic relief of its floor contact reflects a sub-chamber that was emplaced along an angular discordance to its host rock stratigraphy[47]. From north to south, the floor of the Roossenekal sub-chamber first overlies the Steenkampsberg Formation, then transgresses the Houtenbek Formation and finally onlaps the Dullstroom Basalt Formation. The Roossenekal sub-chamber thus attains its maximum thickness in the north and thins towards the south where the CZ eventually terminates against the intrusion floor. The MZ and UZ extend across the entire extent of the two sub-chambers. The MZ in the Roossenekal sub-chamber directly onlaps onto the sedimentary and volcanic floor rocks (Fig. 2).

The second feature relates to the igneous layering, defined by prominent layers termed the Lower, Middle and Upper Mottled Anorthosites (LMA, MMA and UMA), which occur close to the base of the MZ[48]. Although it is widely assumed that the MZ layering abuts the floor contact of country rocks[39,41,42], the Anorthosite Markers do not terminate but drape across the entire Roossenekal and Belfast sub-chambers, including the Stoffberg remnant[48]. The Anorthosite Markers have been traced by the authors along strike at seven field traverses through the basal part of the MZ in both sub-chambers (Fig. 1; Extended Data Figs. 1-4). Field mapping indicates that from north to south the Anorthosite Markers tend to decrease in thickness, without any systematic changes in their textures. Importantly, the presence of the Anorthosite Markers across the entire area indicates that the deposition of MZ cumulates occurred synchronously across the deepest (i.e., Roossenekal sub-chamber base) and shallowest (i.e., Stoffberg remnant summit) parts of the sub-chamber (Fig. 2). This occured despite the elevational distance between these two contrasting depositional places being ~4 km (Fig. 2b). It should be noted that this relationship cannot be due to post-emplacement deformation of the host stratigraphy because the local and regional geology shows no evidence for post-emplacement structural modification, either through faulting or magma emplacement.

Igneous layering in mafic intrusions results from deposition of crystals from the overlying resident melt due to gravity settling[4,49,50] or *in situ* crystallization[9,51,52] onto the chamber floor. This means that in order

to blanket the topographic relief of a temporary floor of the Bushveld chamber with igneous layering (i.e., LMA), the resident melt column must have been thicker than the ~4.0 km height of the Tonteldoos step. The interpretation is supported by a systematic decrease in An-content of plagioclase and Mg-number of orthopyroxene through a ~3.0-km-thick MZ stratigraphy within the Roossenekal sub-chamber, indicating internal differentiation of a resident melt column that was thicker than the crystallised sequence (Fig. 3). The transition to the overlying Pyroxenite Marker is defined by an up to 0.5-km-thick reversal towards more primitive mineral composition (Fig. 3), which has been interpreted as resulting from the mixing of a residual MZ melt with new magma entering the chamber[34,42,44,53,54] and thereby further vertical expansion. Mass balance calculations based on Sr-isotopic data indicate that the residual melt comprised 60-70% of the resulting hybrid magma[34,39], which subsequently crystallized into a >3.0 km thick sequence overlying the Pyroxenite Marker (Fig. 2). If correct, then the residual melt of the MZ must still have been ~2-km-thick prior to the Pyroxenite Marker magma influx, thereby indicating an initial ~5 km thickness of the MZ melt column; resembling earlier estimates based upon thermal modelling of the Bushveld Complex[31]. We concur with previous studies[41,55] that the instantaneous top of the cumulus pile during deposition in this region was gently basinal, with the Stoffberg remnant partially separating the Roossenekal and Belfast sub-chambers. This is best indicated by the concave geometry of the Pyroxenite Marker within the Roossenekal sub-chamber, resulting in this layer being almost 2 km stratigraphically lower at the centre of this sub-chamber, compared to the Stoffberg remnant (Fig. 2). This field evidence implies that the ~1.0 km and ~3.0 km thick MZ in the Roossenekal and Belfast sub-chambers, respectively, formed synchronously from the same interconnected resident melt, as further substantiated by similar An-content of plagioclase at the base of the MZ at both sub-chambers (67.5%[41,56] and 71%[42,43], respectively). A greater thickness of MZ cumulates in the Roossenekal sub-chamber likely relates to a redeposition of crystals inside this depression and/or prevailing crystallization in the deeper parts of the magma chamber, due to a pressure-induced increase in the liquidus temperature of the melt[9,52,57].

Rather than implying that the entire ~5.0 km thick column formed from a single large magma influx, it is proposed that the intrusion progressively grew to its final size (from the Roossenekal subchamber towards the Belfast sub-chamber) through the emplacement of numerous magma influxes, yet over a much shorter time scale than solidification. During this period of repeated injections, each replenishment effectively mixed with the resident melt in the chamber, thereby delaying or impeding the onset of crystallization. Thus, crystallization commenced within a completely filled, large and homogenized magma chamber, which can thereby be modelled as having crystallized as a ‘single pulse’ of magma (Fig. 4a). Our scenario is therefore substantially different from those where the melt crystallization and cumulate pile growth of the MZ occured concurrent with magma chamber replenishment[39]. The scenario conforms better with liquidus phase equilibria predictions for a basaltic parent, like systematic changes in pyroxene assemblages (e.g., Opx-Aug through Opx-Aug-Pig to Aug-Pig)[58] and continuous decreases in both the An-content and Mg-number of cumulus plagioclase and orthopyroxene, respectively (Figs. 3 and 4b). Both the crystallization sequence and mineral compositional trends are successfully reproduced by fractional crystallization of the parental melt using the alphaMELTS software (Fig. 3; Methods, Extended

Data). Such unidirectional evolutionary trends are also inconsistent with models that attribute the formation of the MZ to externally-derived crystal-rich slurries, because these would result in either constant[59] or irregular[22] trends in mineral compositions through the MZ stratigraphy. It is quite conceivable, however, that during protracted fractionation of the MZ resident melt, the chamber may have been further replenished by additional minor magma pulses with or without phenocrysts since minor local reversals in the An-content of plagioclase is descernable within its overall decrease (Fig. 3). In fact, the appearance of the Anorthosite Markers themselves, may be associated with magma chamber replenishments[60]. Such occasional and relatively small magma chamber recharges do not, however, modify our major conclusion with respect to the initial resident melt column thickness, prior to the onset of crystallization at the first anorthosite marker (i.e., LMA in Fig. 2). It was only after a protracted and relatively quiet period of continuous crystallization of the MZ, that a major influx of orthopyroxene-saturated magma incrementally mixed with the magma chamber's resident melt, while concomitantly crystallizing a succession of cumulates both below and above the Pyroxenite Marker (see Thermodynamic modeling in Extended Data).

Implications for the 'big tank' magma chamber paradigm

The 5-km-thick resident melt column that produced the chemically stratified MZ cumulate sequence, including its three prominent anorthosite markers, indicates that during this stage the Bushveld chamber was exceptionally large and entirely molten (Fig. 4). The formation of such a cumulate sequence, at a typical solidification rate for large mafic intrusions (~1 cm/year[49,61]) would take ~300,000 years indicating that the intrusion was also long-lived. These conclusions are at odds with an emerging paradigm that such 'big tank' magma chambers were ephemeral at any given time in Earth's geological history[11,12,14,17,18]. The total volume of resident MZ melt may roughly be estimated as follows. The MZ melt column varied between ~5.0 km in the thicker and, at least, 1.0 km thick in the thinner parts of the intrusion. Based on reconstructions of the lateral extent of the MZ[34], it is estimated that the thicker areas occupied ~70% of the MZ, and the remaining ~30% were thinner zones. The estimated Bushveld Complex area is approximately 100,000 km^3[3,31] and therefore the total volume of the MZ resident melt is ~380,000 km^3 (5 km*70,000 km^2 + 1.0 km*30,000 km^2). This volume is several orders of magnitude larger than the largest ignimbrite/tuff super-eruptions in Earth's history (e.g., Bishop tuff – 600 km^3 and Youngest Toba eruption – up to 13,200 km^3)[25]. It is only comparable to estimates of some of Earth's large igneous provinces, like the Karoo (367,000 km^3)[62] and Afar (350,000 km^3)[26]. Thus, at the MZ stage the Bushveld magma chamber was a repository of an enormous volume of resident melt and may be regarded as a 'big tank' open-system within the Earth's crust. Therefore, a current tendency in modern volcanology[14,17,18] and petrology[19,20,23] to discard the existence of such large and molten magma chambers[4–7] appears to be premature. There is also no compelling reason to believe that 'big tank' magma chambers, such as the 2.05 Ga Bushveld Complex, are restricted to a long-forgotten past of our planet, such as the Precambrian. This is indicated by the 55 Ma Skaergaard intrusion in Greenland whose spectacular chemical stratigraphy indicates that before the onset of crystallization it was a 'big tank' of

crystal-free tholeiitic parent magma up to 4 km in thickness and up to 300 km^3 in volume[63]. It is therefore conceivable that such magma chambers have developed throughout the entire Earth's evolution. Even if some regions of the Earth's crust may behave as giant crystal mushes (e.g., mid-ocean ridges or deep roots of continental arcs)[13,14,16,18], this does not automatically imply that 'big tank' magma chambers are absent from other regions (e.g., stable cratons with layered intrusions)[5–7]. Moreover, since layered intrusions such as the Bushveld Complex are rare throughout geological time[64], it is not surprising that there are currently no active examples of large and molten magma chambers in Earth's crust which can be detected geophysically[27].

Online Content

Any methods, additional references, Nature Research reporting summaries, source data, extended data, supplementary information, acknowledgements, peer review information; details of author contributions and competing interests; and statements of data and code availability are available at

Methods

Map and cross-sections constructions

The regional map was digitised from the 1:250, 000 scale geology maps (2528 Pretoria, and 2530 Barberton, Geological Survey of South Africa) with additional detail from mapping by Van der Merwe (2007), Bevington and Hornsey (2010 – Nuplats Ltd, unpublished mapping), and Latypov and Chistyakova (2021). The geology was overlain on the USGS satellite digital terrane model and wireframes assigned to each lithology. The longitudinal section was drafted with the objective to accurately represent the geological relationships and unit geometries. This was achieved by rotating the map to view it in its true orientation, then digitising the lithologies as a section. This work was undertaken using Micromine™ geological modelling software. The section therefore illustrates the entire stratigraphy and relationships between the Bushveld Complex and its host stratigraphy showing the "as-mapped" relationships and geometries in their correct spatial location. The maps are all in WGS84 Datum, UTM zone 36 South.

MELTS programme, parental melts and its crystallisation sequences

The crystallization of the MZ was modeled using the MELTS algorithm for isobaric fractional crystallization at 2 kbar and FMQ oxygen buffer in steps of 5 °C. The calculations consisted of three major steps. Step 1: identified (by try-and-error) a starting composition (MZ-magma) and reproduced the A-B-C succession of cumulates (Fig. 3). This step reproduced a) the composition trend in Mg-number of orthopyroxene and An-content of plagioclase (considering the trapped liquid shift effect), and the volume proportion of minerals in the observed cumulates and b) the ratio between the volumes of cumulates observed in the stratigraphic column. Step 2: identified an orthopyroxene-saturated (O) magma by try-and-error approach, so that O-magma is more primitive than the MZ-magma, and if not mixed, it produces orthopyroxene at liquidus with a higher Mg-number. Step 3: reproduced the reversals

below the pyroxenite marker (PM), the formation of PM and cumulates above it (A' and B') by gradual mixing of the existing volume of resident magma (R) from stage 1 (~ 30 %) with a new orthopyroxene-saturated magma (O) (see SupplTable S1). Gradually changing the mixing ratio from $O_{10}R_{90}$ to $O_{70}R_{30}$ coupled with concomitant fractional crystallization runs in steps of 1 C° reproduced the mineral assemblage and the variation of Mg-number in orthopyroxene and An-content of plagioclase as observed in zones A' and B' (Fig. 3, and SupplTable 5 and 4B-1 to -7, Extended Data), starting with Mg#-in-orthopyroxene and An reversals below the PM, continuing the reversal trend above the PM and turning to normal fractionation (decreasing) trend towards the top of A' zone. The composition of MZ-, R-, and O-magmas are presented in SupplTable S1 (Extended Data), and the MELTS calculations are summarized in SupplTables S3A, S4A and S5. Detailed calculations are shown in SupplTables S2A, S2B, S2C, S3B, and S4B1 to S4B-7, Extended Data). Complete explanation of the modeling approach can be found in the extended data (Section "Thermodynamic modeling").

Declarations

Data availability

The authors declare that all relevant data are available within the article and its Supplementary Information Files.

Acknowledgements Several versions of this manuscript benefited from the constructive peer reviews by Johan Kruger, Paul Nex, Steve Prevec and Martin Klausen. The study was supported by research grants to R.L. from the National Research Foundation (NRF) and Department of Science and Innovation (DSI)-NRF Centre of Excellence for Integrated Mineral and Energy Resource Analysis (CIMERA) of South Africa. Any opinion, finding and conclusion or recommendation expressed in this contribution is that of the authors and the DSI-NRF CIMERA and NRF do not accept any liability in this regard.

Author Contributions M.M. has done an original mapping of the Anorthosite Markers across the entire study area. R.L., S.C. and R.H. undertook additional field work in this area, including traversing, small-scale mapping and sampling of outcrops as well as conceptualized the original idea and wrote a draft of the paper. R.H. constructed a 3-dimensional geology model of the Eastern limb from which the geological map and longitudinal sections of the study area were produced. G.C. performed thermodynamic modelling and participated in interpretation of data, editing the paper as well as in improving clarity of figures. All co-authors discussed the results and problems and contributed to producing a final draft for peer reviews.

Supplementary Information is available in the online version of the paper.

Competing interests The authors declare no competing interests.

References

1. Daly, R. A. The nature of volcanic action. *Proceedings of the American Academy of Arts and Sciences* **47**, 48–119 (1911).

2. Bowen, N. L. *The evolution of the igneous rocks*. (Oxford University Press, 1928).

3. Wager, L. R. & Deer, W. A. Geological Investigations in East Greenland, Part III: The Petrology of the Skaergaard Intrusion, Kangerdlugssuaq, East Greenland. *Med. Greenland* **105**, 352 (1939).

4. Wager, L. R. & Brown, G. M. *Layered igneous rocks*. (Oliver & Boyd, Edinburgh & London, 1968).

5. Parsons, I. *Origins of Igneous Layering*. vol. 196 (Springer, Dordrecht, 1987).

6. Cawthorn, R. G. *Layered Intrusions*. vol. 15 (Elsevier, Amsterdam, 1996).

7. Charlier, B., Namur, O., Latypov, R. & Tegner, C. *Layered Intrusions*. (Springer Netherlands, 2015).

8. Marsh, B. D. Solidification fronts and magmatic evolution. *Mineral. Mag.* **60**, 5–40 (1996).

9. Campbell, I. H. Fluid dynamic processes in basaltic magma chambers. in *Developments in Petrology* vol. 15 45–76 (Elsevier, 1996).

10. Gudmundsson, A. Magma chambers: formation, local stresses, excess pressures, and compartments. *Journal of Volcanology and Geothermal Research* **237–238**, 19–41 (2012).

11. Glazner, A. F., Coleman, D. S., Gray, W. & Taylor, R. Z. Are plutons assembled over millions of years by amalgamation from small magma chambers? *GSA TODAY* **14**, 4–12 (2004).

12. Coleman, D. S., Gray, W. & Glazner, A. F. Rethinking the emplacement and evolution of zoned plutons: geochronologic evidence for incremental assembly of the Tuolumne Intrusive Suite, California. *Geol* **32**, 433 (2004).

13. Bachmann, O. & Huber, C. The inner workings of crustal distillation columns; the physical mechanisms and rates controlling phase separation in silicic magma reservoirs. *Journal of Petrology* **60**, 3–18 (2019).

14. Cashman, K. V., Sparks, R. S. J. & Blundy, J. D. Vertically extensive and unstable magmatic systems: a unified view of igneous processes. *Science* **355**, eaag3055 (2017).

15. Cooper, K. M. What does a magma reservoir look like? The “crystal’s-eye” view. *Elements* **13**, 23–28 (2017).

16. Edmonds, M., Cashman, K. V., Holness, M. & Jackson, M. Architecture and dynamics of magma reservoirs. *Phil. Trans. R. Soc. A.* **377**, 20180298 (2019).

17. Jackson, M. D., Blundy, J. & Sparks, R. S. J. Chemical differentiation, cold storage and remobilization of magma in the Earth's crust. *Nature* **564**, 405–409 (2018).

18. Sparks, R. S. J. *et al.* Formation and dynamics of magma reservoirs. *Phil. Trans. R. Soc. A.* **377**, 20180019 (2019).

19. Mungall, J. E., Kamo, S. L. & McQuade, S. U–Pb geochronology documents out-of-sequence emplacement of ultramafic layers in the Bushveld Igneous Complex of South Africa. *Nat Commun* **7**, 13385 (2016).

20. Wall, C. J. *et al.* The Stillwater Complex: integrating zircon geochronological and geochemical constraints on the age, emplacement history and crystallization of a large, open-system layered intrusion. *Journal of Petrology* **59**, 153–190 (2018).

21. Robb, S. J. & Mungall, J. E. Testing emplacement models for the Rustenburg Layered Suite of the Bushveld Complex with numerical heat flow models and plagioclase geospeedometry. *Earth and Planetary Science Letters* **534**, 116084 (2020).

22. Yao, Z., Mungall, J. E. & Jenkins, M. C. The Rustenburg Layered Suite formed as a stack of mush with transient magma chambers. *Nat Commun* **12**, 505 (2021).

23. Scoates, J. S. *et al.* Dating the Bushveld Complex: timing of crystallization, duration of magmatism, and cooling of the world's largest layered intrusion and related rocks. *Journal of Petrology* (2021) doi:10.1093/petrology/egaa107.

24. Cawthorn, R. G. The Bushveld Complex, South Africa. in *Layered Intrusions* (eds. Charlier, B., Namur, O., Latypov, R. & Tegner, C.) 517–587 (Springer Netherlands, 2015). doi:10.1007/978-94-017-9652-1_12.

25. Miller, C. F. & Wark, D. A. Supervolcanoes and their explosive supereruptions. *Elements* **4**, 11–15 (2008).

26. Ross, P.-S. *et al.* Mafic volcaniclastic deposits in flood basalt provinces: A review. *Journal of Volcanology and Geothermal Research* **145**, 281–314 (2005).

27. Lundstrom, C. C. & Glazner, A. F. Silicic magmatism and the volcanic–plutonic connection. *Elements* **12**, 91–96 (2016).

28. Bachmann, O. & Bergantz, G. The Magma Reservoirs That Feed Supereruptions. *Elements* **4**, 17–21 (2008).

29. Kruger, W. & Latypov, R. Fossilized solidification fronts in the Bushveld Complex argue for liquid-dominated magmatic systems. *Nat. Commun.* **11**, 2909 (2020).

30. Glazner, A. F. Thermal constraints on the longevity, depth, and vertical extent of magmatic systems. *Geochem Geophys Geosyst* **22**, (2021).

31. Cawthorn, R. G. & Walraven, F. Emplacement and crystallization time for the Bushveld Complex. *J. Petrol.* **39**, 1669–1687 (1998).

32. Naldrett, A. J., Wilson, A., Kinnaird, J., Yudovskaya, M. & Chunnett, G. The origin of chromitites and related PGE mineralization in the Bushveld Complex: new mineralogical and petrological constraints. *Mineral. Deposita* **47**, 209–232 (2012).

33. Finn, C. A., Bedrosian, P. A., Cole, J. C., Khoza, T. D. & Webb, S. J. Mapping the 3D extent of the Northern Lobe of the Bushveld layered mafic intrusion from geophysical data. *Precambrian Res.* **268**, 279–294 (2015).

34. Kruger, F. J. Filling the Bushveld Complex magma chamber: lateral expansion, roof and floor interaction, magmatic unconformities, and the formation of giant chromitite, PGE and Ti-V-magnetitite deposits. *Mineral. Deposita* **40**, 451–472 (2005).

35. Willemse, J. The 'floor' of the Bushveld Igneous Complex and its relationships, with special reference to the Eastern Transvaal. *S. Afr. J. Geol.* **62**, 21–83 (1959).

36. Eales, H. V. Caveats in defining the magmas parental to the mafic rocks of the Bushveld Complex, and the manner of their emplacement: review and commentary. *Mineral. Mag.* **66**, 815–832 (2002).

37. Scoon, R. N. & Mitchell, A. A. Petrogenesis of Discordant Magnesian Dunite Pipes from the Central Sector of the Eastern Bushveld Complex with Emphasis on the Winnaarshoek Pipe and Disruption of the Merensky Reef. *Economic Geology* **99**, 517–541 (2004).

38. Kruger, F. J. & Marsh, J. S. Significance of 87 Sr/ 86 Sr ratios in the Merensky cyclic unit of the Bushveld Complex. *Nature* **298**, 53–55 (1982).

39. Sharpe, M. R. Strontium isotope evidence for preserved density stratification in the main zone of the Bushveld Complex, South Africa. *Nature* **316**, 119–126 (1985).

40. Kruger, F. J. The Sr-isotopic stratigraphy of the western Bushveld Complex. *Trans. geol. Soc. S. Afr.* **97**, 393–398 (1994).

41. Cawthorn, R. G., Lundgaard, K. L., Tegner, C. & Wilson, J. R. Lateral variations in plagioclase compositions, Main Zone, Bushveld Complex, South Africa: Evidence for slow mixing of magmas in basinal structures. *Mineral. mag.* **80**, 213–225 (2016).

42. Setera, J. B. & VanTongeren, J. A. Lateral variability in the Upper Main Zone, Bushveld Complex, owing to directional magma recharge and emplacement from north to south. *Journal of Petrology* **59**, 1763–1786 (2018).

43. Von Gruenewaldt, G. The Main and Upper zones of the Bushveld Complex in the Roossenekal area, eastern Transvaal. *Geological Society of South Africa Transactions* **76**, 53–61 (1973).

44. Nex, P. a. M., Cawthorn, R. G. & Kinnaird, J. A. Geochemical effects of magma addition: compositional reversals and decoupling of trends in the Main Zone of the western Bushveld Complex. *Mineralogical Magazine* **66**, 833–856 (2002).

45. Maier, W. D., Barnes, S.-J. & Groves, D. I. The Bushveld Complex, South Africa: formation of platinum–palladium, chrome- and vanadium-rich layers via hydrodynamic sorting of a mobilized cumulate slurry in a large, relatively slowly cooling, subsiding magma chamber. *Mineral. Deposita* **48**, 1–56 (2013).

46. Cawthorn, R. G. A non-horizontal floor during accumulation of the Bushveld Complex – evidence and implications. *Lithos* **316–317**, 323–329 (2018).

47. Button, A. Stratigraphy and relations of the bushveld floor in the Eastern Transvaal. *South African Journal of Geology* **79**, 3–12 (1976).

48. Merwe, M. V. The occurrence of the critical zone along the exposed southeastern sector of the eastern Bushveld Complex. *South African Journal of Geology* **110**, 617–630 (2007).

49. Morse, S. A. Convection in Aid of Adcumulus Growth. *Journal of Petrology* **27**, 1183–1214 (1986).

50. Irvine, T. N. Magmatic density currents and cumulus processes. *American Journal of Science* **280-A**, 1–58 (1980).

51. McBirney, A. R. & Noyes, R. M. Crystallization and layering of the Skaergaard intrusion. *Journal of Petrology* **20**, 487–554 (1979).

52. Campbell, I. H. Some problems with the cumulus theory. *Lithos* **11**, 311–323 (1978).

53. Cawthorn, R. G., Meyer, P. S. & Kruger, F. J. Major addition of magma at the Pyroxenite Marker in the Western Bushveld Complex, South Africa. *Journal of Petrology* **32**, 739–763 (1991).

54. Vantongeren, J. A. & Mathez, E. A. Incoming magma composition and style of recharge below the Pyroxenite Marker, Eastern Bushveld Complex, South Africa. *Journal of Petrology* **54**, 1585–1605 (2013).

55. Cawthorn, R. G. The Residual or Roof Zone of the Bushveld Complex, South Africa. *Journal of Petrology* **54**, 1875–1900 (2013).

56. Lundgaard, K. L., Tegner, C., Cawthorn, R. G., Kruger, F. J. & Wilson, J. R. Trapped intercumulus liquid in the Main Zone of the eastern Bushveld Complex, South Africa. *Contrib Mineral Petrol* **151**, 352–369 (2006).

57. Jackson, E. D. *Primary textures and mineral associations in the ultramafic zone of the Stillwater complex, Montana*. *Professional Paper* 106 https://pubs.er.usgs.gov/publication/pp358 (1961) doi:10.3133/pp358.

58. Latypov et al. Graphical analysis of the orthopyroxene-pigeonite-augite-plagioclase equilibrium at liquidus temperatures and low pressure. *American Mineralogist* **86**, 547–554 (2001).

59. Roelofse, F. & Ashwal, L. D. The Lower Main Zone in the Northern Limb of the Bushveld Complex—a >1·3 km Thick Sequence of Intruded and Variably Contaminated Crystal Mushes. *Journal of Petrology* **53**, 1449–1476 (2012).

60. Latypov, R. *et al.* Monomineralic anorthosites in layered intrusions are indicators of the magma chamber replenishment by plagioclase-only-saturated melts. *Sci. Rep.* **10**, 3839 (2020).

61. Morse, S. A. The fractional latent heat of crystallizing magmas. *American Mineralogist* **96**, 682–689 (2011).

62. Svensen, H. H., Polteau, S., Cawthorn, G. & Planke, S. Sub-volcanic Intrusions in the Karoo Basin, South Africa. in *Physical Geology of Shallow Magmatic Systems* (eds. Breitkreuz, C. & Rocchi, S.) 349–362 (Springer International Publishing, 2014). doi:10.1007/11157_2014_7.

63. Nielsen, T. F. D. The shape and volume of the Skaergaard intrusion, Greenland: implications for mass balance and bulk composition. *Journal of Petrology* **45**, 507–530 (2004).

64. Smith, W. D. & Maier, W. D. The geotectonic setting, age and mineral deposit inventory of global layered intrusions. *Earth-Science Reviews* **220**, 103736 (2021).

Figures

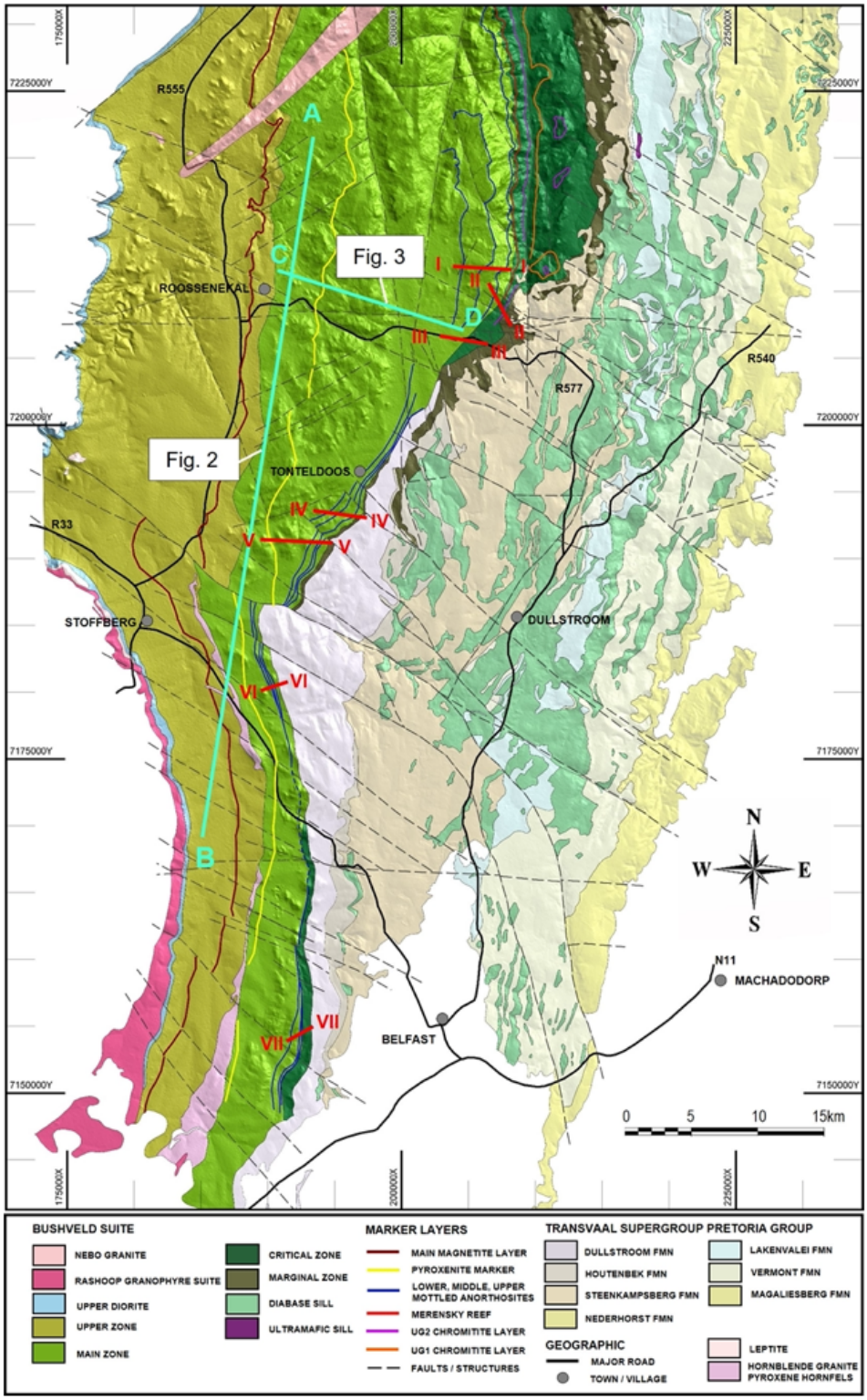

Figure 1

The geological map of the southeastern part of the Bushveld Complex in the Tonteldoos area. The complex transgresses upwards through the Transvaal Supergroup over the northern 35 km of this sector and the floor of the complex steps up by approximately 6 km. The basal part of the Main Zone has three continuous markers layers termed the Lower, Middle and Upper Mottled Anorthosites that extend along the entire area. The position of cross-sections in Figs. 2 and 3 and sevenn major traverses across

Anorthosite Markers (see also Supplementary Data) are indicated. Regional geology digitised from the 1:250000 scale geology maps 2528 Pretoria and 2530 Barberton (Geological Survey of South Africa), with additional detail from mapping by Van der Merwe (2007), Bevington and Hornsey (2010) and Latypov and Chistyakova (2021).

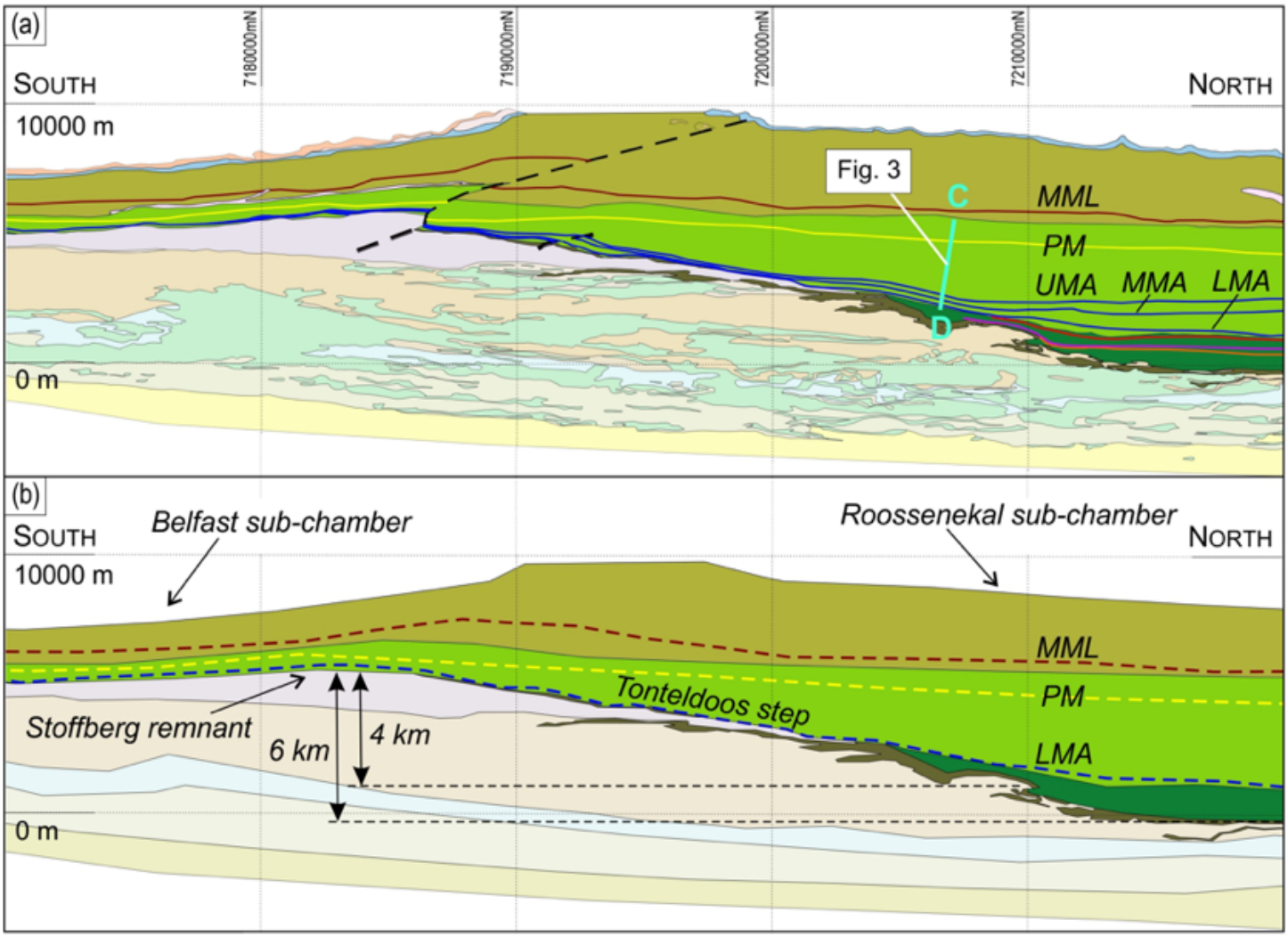

Figure 2

Geological along-strike section of the southeastern part of the Bushveld Complex in the Tonteldoos area. (a) The section goes along the transect line AB in Fig. 1 and looks at -11° towards 270° azimuth. The section has been constructed by rotating the 3D model to view the detailed geology of the complex and its immediate footwall in their true orientation. The section is not vertically or horizontally exaggerated and shows the true lithology morphology. (b) The schematic section prior to faulting that highlights several important features of the complex: (1) the existence of the Roossenekal and Belfast sub-chambers with the intervening Stoffberg remnant of non-deformed host rocks, (2) the ~4-km and ~6-km thick vertical distance between the summit of the Stoffberg remnant with the Lower Mottled Anorthosite and the floor of the Roossenekal sub-chamber, respectively, (3) the concave geometry of the Pyroxenite Marker indicating that instantaneous top of the cumulate pile in two sub-chambers was gently synclinal with regards to the Stoffberg remnant. LMA, Lower Mottled Anorthosite; MMA, Middle Mottled

Anorthosite; UMA, Upper Mottled Anorthosite; PM, Pyroxenite Marker; MML, Main Magnetite Layer. A CD line in (a) shows a position of a cross-section in Fig. 3. Other symbols as in Fig. 1.

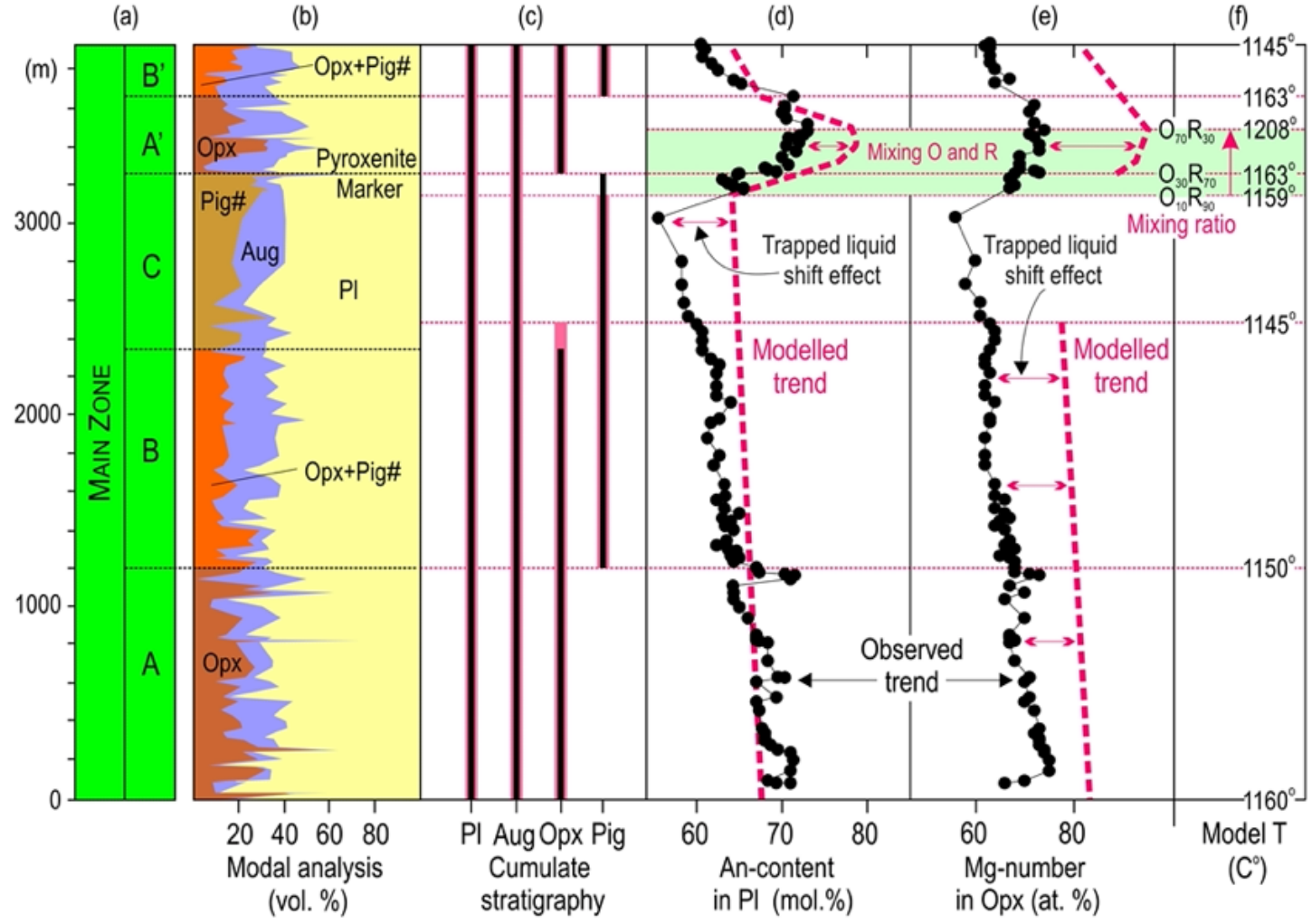

Figure 3

Modal abundances, cumulate stratigraphy and compositional variations of minerals through the Main Zone in the Tonteldoos area of the southeastern part of the Bushveld Complex. The section is approximately along the transect line CD in Figs. 1 and 2. The lower stratigraphy (a-c) is characterized by a systematic crystallization sequence Opx+Aug+Pl (A), Opx+Aug+Pig+Pl (B), and Aug+Pig+Pl (C). The uppermost stratigraphy (a-c) is marked by re-appearance of cumulus Opx at the Pyroxenite Marker so that the crystallization sequence Opx+Aug+Pl (A') and Opx+Aug+Pig+Pl (B') is repeated. The lower stratigraphy (d-e) shows systematic evolutionary trends in composition of plagioclase (decrease in An-content, 100Ca/(Ca+Na)) and orthopyroxene (decrease in Mg-number, 100Mg/(Mg + Fe)). The transition to the Pyroxenite Marker (d-e) is characterized by a gradual compositional reversal towards higher An-content of plagioclase and Mg-number of orthopyroxene. All compositional data in (a-e) are from Gruenewaldt43 and are summarized in Supplementary Data Table 1. The trapped liquid shift in composition of Mg-number in orthopyroxene and An-content in plagioclase represent the re-equilibration of the minerals with the trapped liquid during cooling at the post-cumulate stage. The modelling results

are explained in the electronic appendix (Section “Thermodynamic modelling”), summarized in SuplTables S3A, S4a and S5, and presented in detail in SupplTables S3B and S4B-1 to S4B-7). O, orthopyroxene-saturated magma; R, resident melt; Pl, plagioclase; Opx, orthopyroxene; Aug, augite; Pig#, inverted pigeonite.

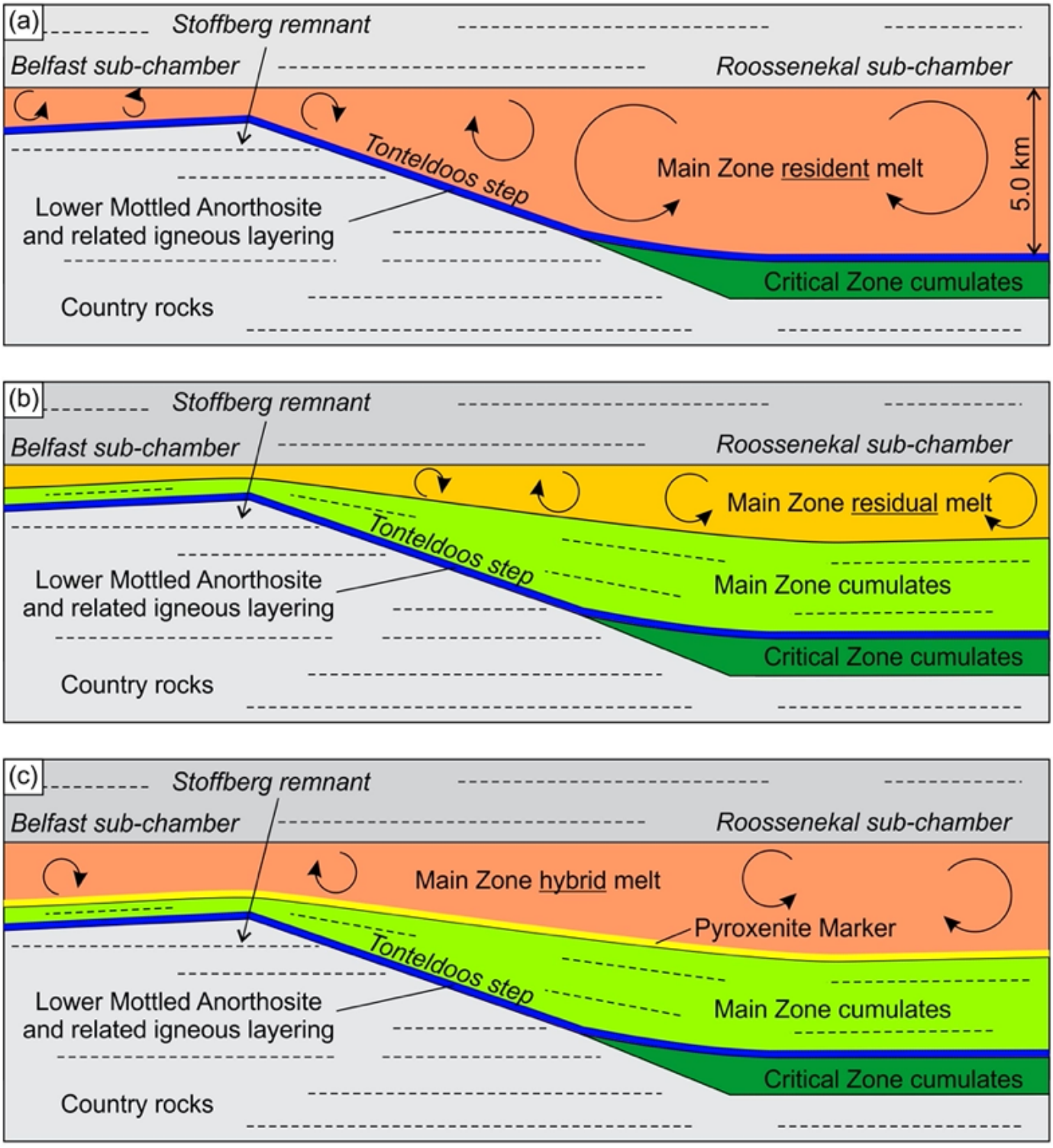

Figure 4

Model for the proposed crystallization history of the Main Zone in the Tonteldoos area of the southeastern part of the Bushveld Complex. (a) By onset of crystallization, the MZ resident melt column reaches a total thickness of about 5 km. This resulted in simultaneous deposition of the Lower Mottle Anorthosite along the entire extent of the Roossenekal and Belfast sub-chambers, including the Tonteldoos step and Stoffberg remnant. (b) Internal crystallization and differentiation of the MZ resident melt from the base upwards produced a continuous sequence of chemically-stratified cumulate rocks. The instantaneous top of the cumulate pile in the chamber was gently synclinal with the Stoffberg remnant separating two sub-chambers. (c) The mixing of the MZ residual melt with a new inflowing melt resulted in the formation of the MZ hybrid melt that produced the laterally extensive Pyroxenite Marker with an associated reversal in mineral compositions. The total volume of resident melt before onset of crystallization is estimated at >380,000 km3 which allows to classify the Bushveld chamber as a ‘big tank’ open-system within the Earth’s crust. The figure is not to scale for illustration purposes.

Supplementary Files

This is a list of supplementary files associated with this preprint. Click to download.

- LatypovfieldobservationsUTM36S.txt
- HornseyBevingtonfieldobservationsUTM36S.zip
- LatypovChistyakovafieldobservationsUTM36S.zip
- 20211005LatypovetalFieldXWPTGeologyObservationsUTM36S.xlsx
- ExtendedData22Nov2021.docx
- SupplTableS1CompositionsofmodeledMZRandOmagmas.xlsx
- SupplTableS2AFractionalcrystallizationofdryMORBtholeiiteat2kbar.xlsx
- SupplTableS2BFractionalcrystallizationofwetMORBtholeiiteat2kbar.xlsx
- SupplTableS2CRmagmamixedwithMORBwetfractcrystalat2kbar.xlsx
- SupplTableS2DB2magmafractionalcrystallizationat2kbar.xlsx
- SupplTableS3AMineralassemblagefractcrystalat2kbarsMZmagma.xlsx
- SupplTableS3BDetailedfractionalcrystallizationofMZmagmaat2kbar.xlsx
- SupplTableS4ADetailedfractionalcrystallizationofOmagmaat2kbar.xlsx
- SupplTableS4B1FractionalcrystallizationofthemixO10R90.xlsx
- SupplTableS4B2FractionalcrystallizationofthemixO20R80.xlsx
- SupplTableS4B3FractionalcrystallizationofthemixO30R70.xlsx
- SupplTableS4B4FractionalcrystallizationofthemixO40R60.xlsx
- SupplTableS4B5FractionalcrystallizationofthemixO50R50.xlsx
- SupplTableS4B6FractionalcrystallizationofthemixO60R40.xlsx
- SupplTableS4B7FractionalcrystallizationofthemixO70R30.xlsx

- SupplTableS5SummaryofPMmodellingresults.xlsx